I&EC research
Industrial & Engineering Chemistry Research

Article

pubs.acs.org/IECR

Continuous-Flow Precipitation of Hydroxyapatite at 37 °C in a Meso Oscillatory Flow Reactor

Filipa Castro,*[,†] António Ferreira,[†,‡] Fernando Rocha,[‡] António Vicente,[†] and José António Teixeira[†]

[†]Institute for Biotechnology and Bioengineering (IBB), Centre for Biological Engineering, University of Minho, Campus de Gualtar, 4710-057 Braga, Portugal

[‡] Laboratory for Process, Environmental and Energy Engineering (LEPAE), Faculty of Engineering, University of Porto, Rua Roberto Frias, s/n, 4200-465 Porto, Portugal

ABSTRACT: Continuous-flow precipitation of hydroxyapatite (HAp) was investigated in a meso oscillatory flow reactor (meso-OFR) and in a scaled-up meso-OFR, obtained by associating in series eight vertical meso-ORFs. Experiments were carried out under near-physiological conditions of temperature and pH, using fixed frequency (f = 0.83 Hz) and amplitude (x_0 = 4.5 mm), and varying the residence time from 0.4 to 6.7 min. It has been shown that the mean particle size and the aggregation degree of the prepared HAp particles decrease with decreasing residence time. HAp nanoparticles with a mean size (d_{50}) of 77 nm, narrow size distribution, and uniform morphology were obtained at the lowest residence times, τ = 0.4 and 3.3 min in the meso-OFR and the scaled-up meso-OFR, respectively. These results show the capability of the meso-OFR and the scaled-up meso-OFR for continuous production of uniform HAp nanoparticles, while also confirming the possibility of OFR scale-up by in series association of individual OFRs.

1. INTRODUCTION

Hydroxyapatite (HAp), $Ca_5(PO_4)_3OH$, has been extensively used in bone replacement applications due to its biocompatibility, bioactivity, and osteoconductivity.[1] In this context, it is desirable that HAp crystals meet specific requirements, such as high specific surface area (favored by small crystal size), narrow size distribution, and high purity, in order to optimize bone-related cell growth around them.[1,2]

Traditional stirred tank batch reactors for synthetic production of HAp provide only limited amounts of material, and crystallization conditions may change during multiple syntheses.[3] In this kind of system, low mixing efficiency and wide residence time distributions lead to a heterogeneous distribution of supersaturation in the reaction medium, thus affecting the crystal size distribution and chemical purity of the precipitated particles. The problem is magnified as the scale of operation increases, since the control of mixing is very difficult in large vessels,[4] and can be particularly pronounced in fast precipitation systems owing to the very fast reaction kinetics.[5]This can lead to problems in achieving consistent product specifications.[3] Even small differences in stoichiometry, morphology, or size may affect the chemical, biological, and physical behaviors of the material.[6] On one hand, scale-up is necessary to increase production rate, and on the other hand the science of reactive precipitation makes it difficult to apply precipitations to industrial scale batch operations under well-defined and reproducible conditions.

Continuous operation offers significant advantages in terms of process and costs.[3,7,8] It allows more efficient use of reagents, solvents, energy, and space while minimizing the production of waste materials and reactor downtime for reactor maintenance and cleaning. Further, it affords the advantage of enhanced reproducibility of results because all material crystallizes under uniform conditions, resulting in the formation of crystals with consistent properties.[3] In addition, continuous operations allow higher productivity and permit the continuous variation of the chemical composition of the reaction medium.

The application of periodic fluid oscillations to a cylindrical column containing evenly spaced orifice baffles is the basic concept of an oscillatory flow reactor (OFR).[9] The OFR can be operated batchwise or continuously in horizontal or vertical tubes. The fluid is typically oscillated in the axial direction by means of diaphragms, bellows, or pistons, at one or both ends of the tube, developing an efficient mixing mechanism (oscillatory flow mixing) where fluid moves from the walls to the center of the tube with intensity controlled by the oscillation frequency and amplitude.[9−11] In recent years, the study of oscillatory flow mixing within OFRs has increasingly been applied to various industrial processes, such as suspension polymerization, crystallization, paint dispersion, flocculation, and fermentation.[12−17]

In this work, a simple apparatus for the continuous preparation of HAp nanoparticles under near-physiological conditions of temperature and pH is presented. Continuous-flow precipitation of HAp was performed in a meso oscillatory flow reactor (meso-OFR) and in the scaled-up meso-OFR, which were suitable for continuous high throughput screening due to their small volumes (milliliters). HAp precipitation was carried out at 37 °C, for a mixing molar ratio Ca/P of 1.33, and at different residence times τ = 0.9 and 0.4 min for the meso-OFR and τ = 6.7 and 3.3 min for the scaled-up meso-OFR. Characteristics of the prepared powders (purity, size, size

Received: March 4, 2013
Revised: June 4, 2013
Accepted: June 29, 2013
Published: June 29, 2013

ACS Publications © 2013 American Chemical Society

dx.doi.org/10.1021/ie400710b | *Ind. Eng. Chem. Res.* 2013, 52, 9816−9821

distribution, and morphology) were evaluated for all the operating conditions.

2. MATERIALS AND METHODS

2.1. Description of the Experimental Setup. The meso-OFR consists of a 35 cm long and 4.4 mm internal diameter glass jacketed tube provided with smooth periodic cavities (SPC), with an average baffle spacing of 13 mm and a baffle thickness of 6 mm.[9,18,19] The diameter of the constricted zone (baffle internal diameter) is 1.6 mm, leading to a baffle free area of 13%.[9] The reactor has an approximate volume of 4 mL.

HAp precipitation was first carried out in the meso-OFR operated continuously in a vertical tube (see Figure 1).

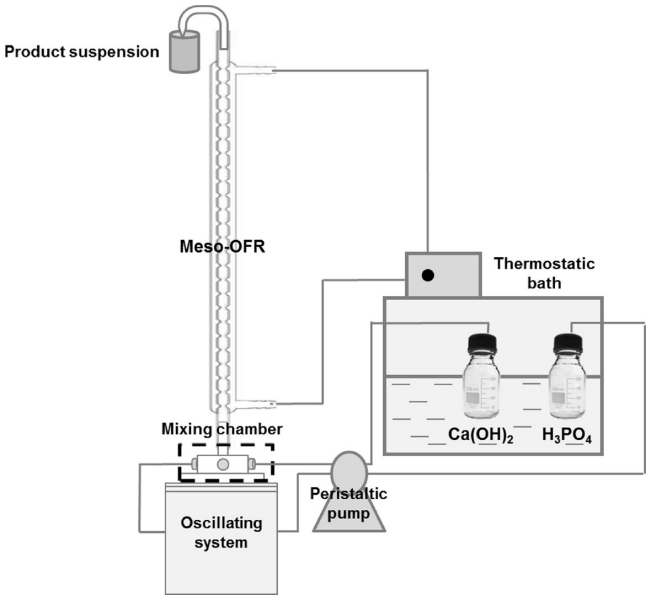

Figure 1. Experimental apparatus for the continuous-flow precipitation of HAp.

HAp precipitation was then carried out in the scaled-up meso-OFR. For this, eight meso-OFRs were positioned in series, with each meso-OFR placed vertically (see Figure 2).

For both experimental apparatuses, the fluid was oscillated using a piston moved by a stirring motor (CAT R100C). The oscillating system was custom-built. Based on preliminary experiments, the oscillation amplitude (x_0) and frequency (f) were fixed at 4.5 mm and 0.83 Hz, respectively. The value of the amplitude corresponds to the center-to-peak amplitude, and the measurements were performed in the tube without constrictions. Reactants were fed into the setups by means of a peristaltic pump (ISMATEC IPS 8, Switzerland). The temperature of the reactants and the temperature inside the meso-OFRs were regulated by a thermostatic bath maintained at 37 °C.

2.2. Powder Preparation. HAp was synthesized by the mixing of a saturated calcium hydroxide (Sigma-Aldrich, 95%) aqueous solution and an orthophosphoric acid (Mallinckrodt, 85%) aqueous solution at 37 °C, with a mixing molar ratio Ca/P = 1.33. This mixing molar ratio was defined in order to obtain the desired product, e.g., HAp, under conditions that promote the survival of bone-related cells, e.g., physiological conditions of pH and temperature. After several preliminary experiments, the mixing molar ratio Ca/P = 1.33 was confirmed as the one that allowed obtaining the desired product at near-physiological

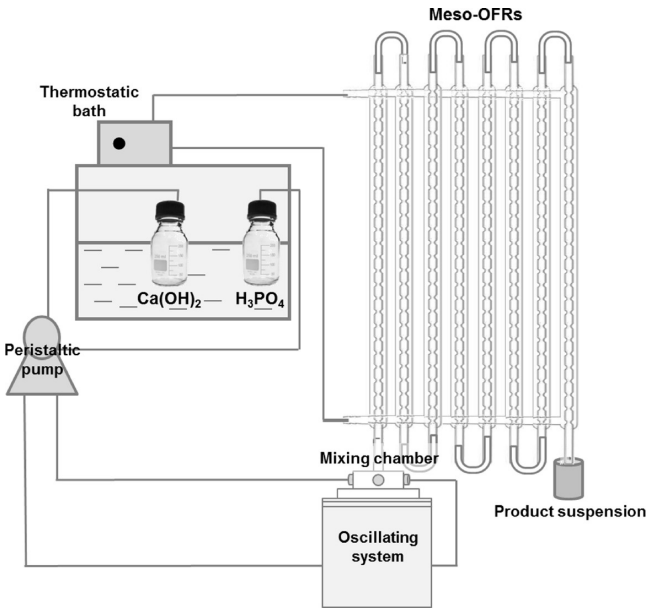

Figure 2. Experimental apparatus for the scale-up of the continuous-flow precipitation of HAp.

conditions of pH and temperature. A 0.5 L volume of both reactants was prepared with ultrapure water (Milli Q water, resistivity of 18.2 MΩ/cm at 25 °C), and their ionic force was adjusted by the addition of 6 mL of 4 mol·L^{-1} potassium chloride (Mallinckrodt, 99.8%) solution. To facilitate the dissolution of calcium hydroxide, the solution was agitated in a closed vessel for 24 h at 500 rpm and at 25 °C, as its solubility decreases with temperature increase.[20] Then, both reactants were heated and kept at 37 °C.

According to preliminary experiments, f = 0.83 Hz and x_0 = 4.5 mm were found to be the best conditions for promoting a fast mixing and a more homogeneous reaction medium, being thus defined as the operating conditions. Further, HAp precipitation was carried out at different residence times in both the meso-OFR and the scaled-up meso-OFR. The operating conditions are presented in Table 1.

Table 1. Operating Conditions for the Continuous-Flow Precipitation of HAp in the Meso-OFR and in the Scaled-Up Meso-OFR

reactor	liquid flow rate (mL/min)	number of meso-OFRs	total vol (mL)	τ (min)
meso-OFR	4.5	1	≈4	0.9
	9.0	1	≈4	0.4
scaled-up meso-OFR	4.5	8	≈30	6.7
	9.0	8	≈30	3.3

Temperature (inoLab, WTW) and pH (SenTix Mic-D, WTW) were measured at different time intervals at the outlet of the meso reactor. The pH electrode was calibrated with two buffer solutions at pH 7.00 and 10.00 at 25 °C.

Samples were collected after approximately two to three residence times, until pH stabilization was achieved.

2.3. Powder Characterization. Samples were withdrawn at the outlet of the meso reactor, centrifuged (at 1500 rpm for 5 min), washed twice with ultrapure water, and conserved in pure ethanol (99.8%), which stops the solid−liquid reaction.[21] The

dx.doi.org/10.1021/ie400710b | Ind. Eng. Chem. Res. 2013, 52, 9816−9821

powders obtained were then characterized by X-ray diffraction (XRD; PanAlytical X'Pert PRO Alfa-1 diffractometer with λ Cu Kα = 1.540 56 Å), Fourier transform infrared spectroscopy (FTIR; Bomem MB-154S), and scanning electron microscopy (SEM; FEI Quanta 400FEG ESEM/EDAX Genesis X4M with an accelerating voltage of 15 kV and 20 kV), where samples were covered by a 10 nm layer of gold. For particle size distribution, suspensions were collected at the end of each experiment and directly analyzed by laser diffraction (LS 230, Beckman Coulter). The final precipitate was also dried and weighed for the estimation of the mass of the crystals obtained.

3. RESULTS AND DISCUSSION

3.1. Important Parameters in the Precipitation of HAp. pH is an important parameter in determining the likelihood of the formation of calcium phosphate phases.[22] The influence of pH on the formation of calcium phosphates is linked to the properties of phosphate-containing solutions. Due to the triprotic equilibrium in these systems, variations in pH alter the relative concentrations of the four protonated forms of phosphoric acid and thus both the chemical composition and the amount of the CaP formed by direct precipitation.[23]

In the present work, experiments were conducted under near-physiological conditions of temperature and pH (Table 2), which is particularly important when preparing HAp for medical purposes.

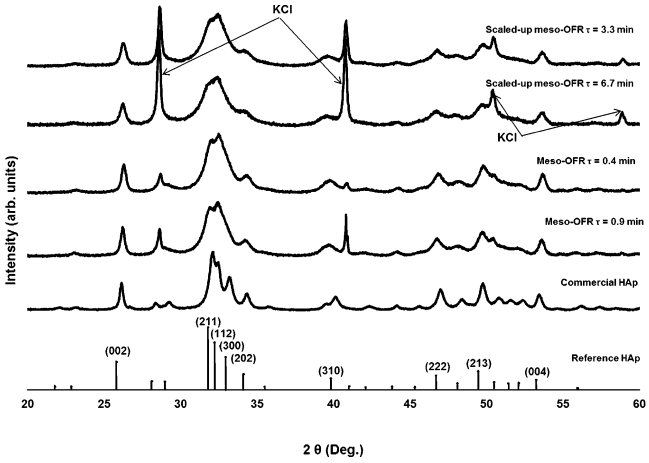

Figure 3. XRD patterns of the particles produced in the meso-OFR and scaled-up meso-OFR operated continuously at different operating conditions.

Table 2. Parameters Measured during Continuous-Flow Precipitation of HAp in the Meso-OFR and in the Scaled-Up Meso-OFR, for Different Operating Conditions

reactor	τ (min)	pH	precipitate (mg/mL)
meso-OFR	0.9	6.90	0.87
	0.4	7.10	0.93
scaled-up meso-OFR	6.7	6.63	0.80
	3.3	6.65	0.83

As already mentioned, it is important to follow specific criteria for pH and temperature in order to promote more conductive conditions for the survival of bone-related cells.[2] Furthermore, from a thermodynamic point of view, these conditions favor the precipitation of HAp, since at 37 °C and pH between 4 and 12, HAp is the most stable calcium phosphate salt.[24] Concerning the quantity of the precipitate obtained, results presented in Table 2 show that the mass of precipitate prepared per milliliter is similar for all operating conditions.

3.2. Continuous-Flow HAp Precipitation. *3.2.1. Phase Identification.* The XRD analysis of the prepared powders (see Figure 3) revealed no secondary phases besides the apatitic phase, for all the operating conditions studied. XRD patterns of the different powders obtained match well the XRD pattern of a reference HAp (JCPDS 9-0432) and a commercial HAp (Spectrum, minimum 40 meshes). However, broadening and overlap of the peaks are observed, being more pronounced in the diffraction pattern of the particles produced in the scaled-up meso-OFR. This may imply small crystallites and low crystallinity, which is similar to natural bone.[25] Peaks assigned to KCl (namely at 28° 2θ and 40.5° 2θ) are also exhibited, especially in the diffraction patterns of the particles prepared in the scaled-up meso-OFR. This may be explained by the occlusion of KCl present in the mother liquor, which could have been trapped in the aggregates and crystallized at the drying step. KCl peaks are less detected for the lowest residence times.

It can also be seen that there is a slight shift between the XRD patterns of the prepared powders and the XRD pattern of the reference HAp. This is probably due to the experimental conditions under which XRD analysis was performed, since a slight shift is also visible in the diffraction pattern of the commercial HAp.

According to Figure 4, FTIR spectra exhibit stretching and bending vibrations of the phosphate, PO_4^{3-}, and the hydroxyl,

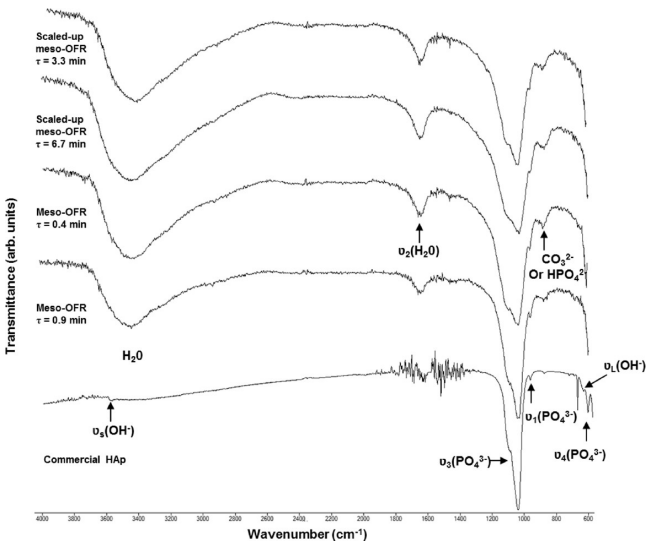

Figure 4. FTIR spectra of the particles produced in the meso-OFR and scaled-up meso-OFR operated continuously at different operating conditions.

OH^-, functional groups, characteristic of a typical apatite structure.[26] However, it is difficult to detect the peak related to the υ_4 bending mode of PO_4^{3-}, and the peaks assigned to the vibrational mode (around 630 cm^{-1}) and stretching mode (around 3571 cm^{-1}) of OH^- are not well resolved. Concerning the peak assigned to the stretching mode of OH^-, this can be due to the overlap with the broad band (from approximately 3700 to 3000 cm^{-1}) of the adsorbed water on HAp particles.[27] A second peak assigned to adsorbed water is also observed at

dx.doi.org/10.1021/ie400710b | Ind. Eng. Chem. Res. 2013, 52, 9816−9821

1643 cm^{-1} (bending mode, υ_2). The presence of adsorbed water on the HAp prepared particles can be explained by the low drying temperature (60 °C) and the absence of a ripening (aging) treatment.[18,19,28] In addition, the presence of a peak (around 875 cm^{-1}) assigned to the vibrational frequencies of carbonate (CO_3^{2-}) or hydrogen phosphate (HPO_4^{2-}) ions[17,20] suggests the formation of a carbonated HAp or calcium-deficient HAp.

3.2.2. Particle Size, Size Distribution, and Morphology. According to Figures 5 and 6 (obtained from the conversion of the particle size distribution in volume) and Tables 3 and 4 (obtained from the conversion of the particle size distribution in volume), the as-prepared powders consist of a population of primary particles in the nanometer range and a population of micrometer-sized aggregates that, given the considerable difference in size, could be separated. Aggregates probably result from the aggregation of primary nanoparticles, since small particles possess a high surface-area-to-volume ratio, resulting in a high surface tension which they tend to lower by adhering to one another.[29] Further, the peak observed at 1000 μm (see Figure 5) is probably due to the presence of air bubbles in the suspensions analyzed. Results also show that the mean size and the aggregation degree of the as-prepared particles increase with increasing residence time. On the basis of Figure 6 and Table 4, HAp particles with a mean size (d_{50}) of 77 nm were obtained at the residence times τ = 0.4 and 3.3 min, for the meso-OFR and the scaled-up meso-OFR, respectively. Indeed, for higher liquid flow rates, Reynolds numbers are higher and mixing efficiency is enhanced. This results in a more homogeneous reaction medium and therefore in a more homogeneous distribution of supersaturation, thus affecting the size distribution of the particles.[30−33] When compared with the commercial HAp particles (Spectrum, minimum 40 meshes) originally submitted to granulometric separation, the HAp particles prepared at the lowest residence times (τ = 0.4 min for the meso-OFR and τ = 3.3 min for the scaled-up meso-OFR) have a lower mean size (d_{50}) and a narrower size distribution (Table 4). However, it is very important to underline that the particles produced were directly obtained from the system without thermal treatment and without granulometric separation.

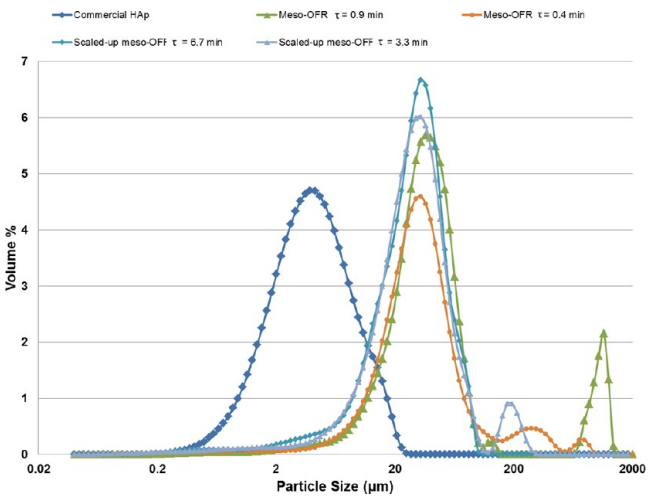

Figure 5. Particle size distribution in volume of particles produced in the meso-OFR and scaled-up meso-OFR operated continuously at different operating conditions.

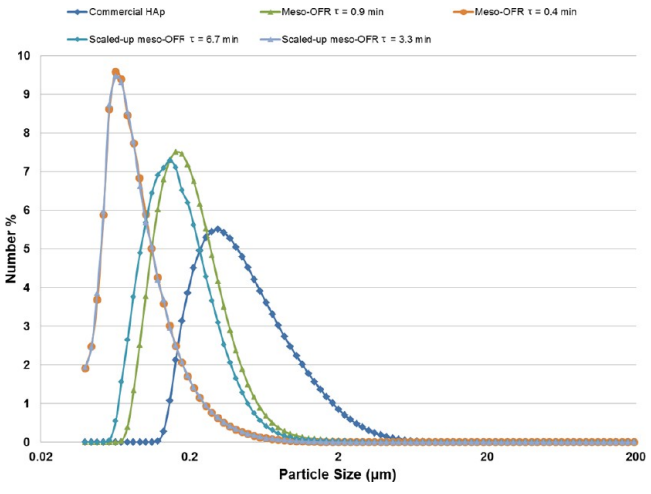

Figure 6. Particle size distribution in number of particles produced in the meso-OFR and scaled-up meso-OFR operated continuously at different operating conditions.

Figure 7 shows two types of particles for the residence times τ = 0.9 and 6.7 min, for the meso-OFR and the scaled-up meso-OFR, respectively: rod-shaped and plate-shaped. Regarding particles produced at τ = 0.4 and 3.3 min, for the meso-OFR and the scaled-up meso-OFR, respectively, the morphology seems more uniform and particles look to be mostly rod-shaped. In both cases, rod-shaped particles present a size around 100 nm long and 20 nm wide. As already mentioned, mixing is more efficient for higher Reynolds numbers, providing more homogeneous reaction conditions,[30,32,33] and improving thus the monodispersity of synthesized nanoparticles.[34−37]

Based on the above-mentioned results, the feasibility of the meso-OFR and the scaled-up meso-OFR was demonstrated for the continuous production of uniform HAp nanoparticles. In both the meso-OFR and the scaled-up meso-OFR operated continuously, single-phase HAp nanoparticles with a mean size (d_{50}) of 77 nm and a narrow size distribution were obtained.

4. CONCLUSION

Continuous-flow precipitation of HAp was investigated in a meso-OFR and in a scaled-up meso-OFR. Calcium-deficient and/or carbonated HAp nanoparticles were successfully produced in both reactors. The influence of the residence time on HAp particle size and size distribution was also studied. For both reactors, it was found that the mean particle size and the aggregation degree of the particles decrease with the decrease of the residence time. In addition, HAp particles more uniform in size were precipitated for both the meso-OFR and the scaled-up meso-OFR at the lowest residence times. Single-phase HAp nanoparticles with a mean size (d_{50}) of 77 nm and a narrow size distribution were obtained in both the meso-OFR and the scaled-up meso-OFR. Furthermore, the precipitated HAp particles show improved quality, namely in terms of size and size distribution, when compared with a commercial HAp powder. It is important to note that, unlike the commercial powder that was previously subjected to granulometric separation, samples obtained in this study were not submitted to further treatment. Thus, the proposed scaled-up meso-OFR may be useful as a high throughput screening tool, namely for performing reactions which require longer reaction times.

dx.doi.org/10.1021/ie400710b | Ind. Eng. Chem. Res. 2013, 52, 9816−9821

Table 3. Parameters of the Particle Size Distribution (in Volume) of Powders Produced in the Meso-OFR and Scaled-Up Meso-OFR Operated Continuously at Different Operating Conditions[a]

			particle size (μm)			
reactor	operation type	τ (min)	d_{10}	d_{50}	d_{90}	span
meso-OFR	continuous flow	0.9	14.68	38.31	110.1	2.49
	continuous flow	0.4	12.75	32.88	93.98	2.47
scaled-up meso-OFR	continuous flow	6.7	10.07	30.18	59.12	1.60
	continuous flow	3.3	9.62	27.60	62.74	1.92
commercial HAp		–	1.29	3.72	10.19	2.39

[a] d_{10}, 10% of the particles are smaller than this value; d_{50}, 50% of the particles are smaller than this value; d_{90}, 90% of the particles are smaller than this value; span, width of the distribution based on the 10, 50, and 90% quantiles.

Table 4. Parameters of the Particle Size Distribution (in Number) of Powders Produced in the Meso-OFR and Scaled-Up Meso-OFR Operated Continuously at Different Operating Conditions[a]

			particle size (μm)			
reactor	operation type	τ (min)	d_{10}	d_{50}	d_{90}	span
meso-OFR	continuous flow	0.9	0.106	0.183	0.389	1.55
	continuous flow	0.4	0.050	0.077	0.171	1.57
scaled-up meso-OFR	continuous flow	6.7	0.087	0.154	0.332	1.59
	continuous flow	3.3	0.049	0.077	0.172	1.60
commercial HAp		–	0.19	0.40	1.22	3.03

[a] d_{10}, 10% of the particles are smaller than this value; d_{50}, 50% of the particles are smaller than this value; d_{90}, 90% of the particles are smaller than this value; span, width of the distribution based on the 10, 50, and 90% quantiles.

In summary, the present study demonstrates the capabilities of a meso-OFR and a scaled-up meso-OFR for the continuous production of HAp nanoparticles, taking advantage of both oscillatory flow mixing and continuous operation.

AUTHOR INFORMATION

Corresponding Author

*E-mail: fcastro@deb.uminho.pt. Tel.: +351.253.604400. Fax: +351.253.678986.

Notes

The authors declare no competing financial interest.

REFERENCES

(1) He, Q. J.; Huang, Z. L. *Cryst. Res. Technol.* **2007**, *42*, 460−465.

(2) Kumta, P. N.; Sfeir, C.; Lee, D.-H.; Olton, D.; Choi, D. *Acta Biomater.* **2005**, *1*, 65−83.

(3) Lawton, S.; Steele, G.; Shering, P.; Zhao, L.; Laird, I.; Ni, X.-W. *Org. Process Res. Dev.* **2009**, *13*, 1357−1363.

(4) Jongen, B. N.; Donnet, M.; Bowen, P.; Lemaître, J.; Hofmann, H.; Schenk, R.; Hofmann, C.; Aoun-Habbache, M.; Guillemet-Fritsch, S.; Sarrias, J.; Rousset, A.; Viviani, M.; Buscaglia, M. T.; Buscaglia, V.;

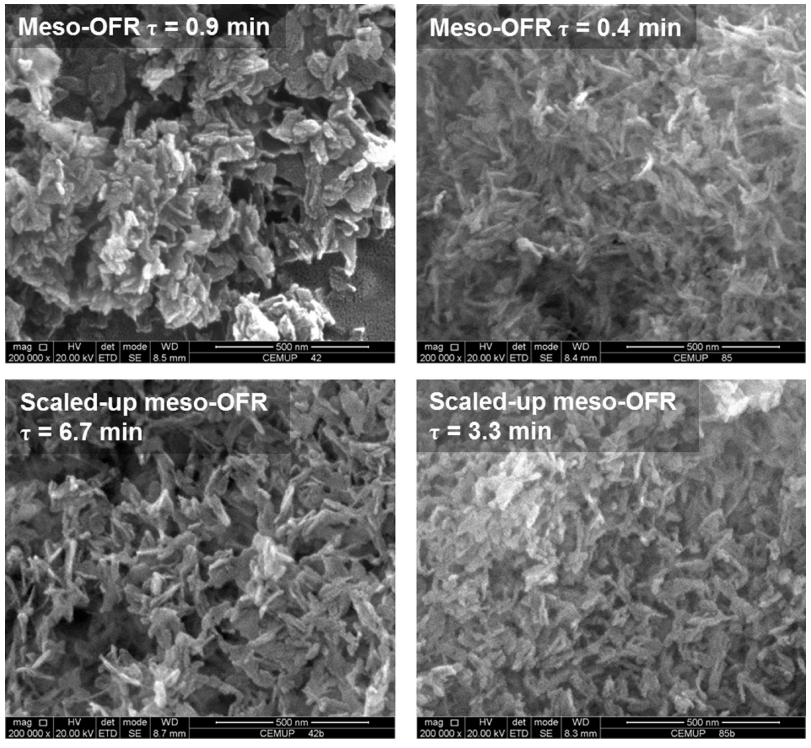

Figure 7. SEM images of particles produced in the meso-OFR and scaled-up meso-OFR operated continuously at different operating conditions.

Nanni, P.; Testino, A.; Herguijuela, J. R. *Chem. Eng. Technol.* **2003**, *26*, 303−305.
(5) Jones, A.; Rigopoulos, S.; Zauner, R. *Comput. Chem. Eng.* **2005**, *29*, 1159−1166.
(6) Tadic, D.; Peters, F.; Epple, M. *Biomaterials* **2002**, *23*, 2553−9.
(7) Mcmullen, J. P.; Jensen, K. F. *Org. Process Res. Dev.* **2010**, *14*, 1169−1176.
(8) Lopes, A. M.; Silva, D. P.; Vicente, A. A.; Pessoa-Jr, A.; Teixeira, J. A. *J. Chem. Technol. Biotechnol.* **2011**, *86*, 1159−1165.
(9) Reis, N. M. F. *Novel Oscillatory Flow Reactors for Biotechnological Applications*. Thesis, University of Minho, Braga, Portugal, 2006.
(10) Ni, X.; Sommer, Y.; Gélicourt, D.; Neil, J.; Howes, T. *Chem. Eng. J.* **2002**, *85*, 17−25.
(11) Ni, X.; Jian, H.; Fitch, A. W. *Chem. Eng. Sci.* **2002**, *57*, 2849−2862.
(12) Chew, C. M.; Ristic, R. I. *AIChE J.* **2005**, *51*, 1576−1579.
(13) Ristic, R. *Chem. Eng. Res. Des.* **2007**, *85*, 937−944.
(14) Ni, X.; Gao, S.; Cumming, R. H.; Pritchard, D. W. *Chem. Eng. Sci.* **1995**, *50*, 2127−2136.
(15) Ni, X.; Johnstone, J. C.; Symes, K. C.; Grey, B. D.; Bennett, D. C. *AIChE J.* **2001**, *47*, 1746−1757.
(16) Harvey, A.; Mackley, M. R.; Reis, N.; Teixeira, J. A.; Vicente, A. A. *30th Conference of the SSCHE, Tatranské Matliare, Slovakia* [CD-ROM]; Slovak Society of Chemical Engineering: Bratislava, Slovakia, 2003; pp 26−30.
(17) Ni, X.; Murray, K.; Zhang, Y.; Bennett, D.; Howes, T. *Powder Technol.* **2002**, *124*, 281−286.
(18) Reis, N.; Vicente, A. A.; Teixeira, J. A.; Mackley, M. R. *Chem. Eng. Sci.* **2004**, *59*, 4967−4974.
(19) Reis, N.; Harvey, A.; Mackley, M. R.; Vicente, A. A.; Teixeira, J. A. *Chem. Eng. Res. Des.* **2005**, *83*, 357−371.
(20) Johannsen, K.; Rademacher, S. *Acta Hydrochim. Hydrobiol.* **1999**, *27*, 72−78.
(21) Bernard, L.; Freche, M.; Lacout, J.; Biscans, B. *Chem. Eng. Sci.* **2000**, *55*, 5683−5692.
(22) Wang, L.; Nancollas, G. H. *Chem. Rev.* **2008**, *108*, 4628−69.
(23) Lynn, A. K.; Bonfield, W. *Acc. Chem. Res.* **2005**, *38*, 202−207.
(24) Elliot, J. C. *Structure and Chemistry of the Apatites and Other Calcium Orthophosphates*; Elsevier: Amsterdam, 1994.
(25) Meskinfam, M.; Sadjadi, M. S.; Jazdarreh, H. *Int. J. Chem. Biol. Eng.* **2012**, *6*, 192−195.
(26) Koutsopoulos, S. *J. Biomed. Mater. Res.* **2002**, *62*, 600−612.
(27) Ma, M.-G.; Zhu, J.-F. *Eur. J. Inorg. Chem.* **2009**, 5522−5526.
(28) Osaka, A.; Miura, Y.; Takeuchi, K.; Asada, M.; Takahashi, K. *J. Mater. Sci.: Mater. Med.* **1991**, *2*, 51−55.
(29) Luque de Castro, M. D.; Priego-Capote, F. *Ultrason. Sonochem.* **2007**, *14*, 717−24.
(30) Wang, K.; Wang, Y. J.; Chen, G. G.; Luo, G. S.; Wang, J. D. *Ind. Eng. Chem. Res.* **2007**, *46*, 6092−6098.
(31) Aimable, A.; Jongen, N.; Testino, A.; Donnet, M.; Lemaître, J.; Hofmann, H.; Bowen, P. *Chem. Eng. Technol.* **2011**, *34*, 344−352.
(32) Günther, A.; Jensen, K. F. *Lab Chip* **2006**, *6*, 1487−503.
(33) Mersmann, A. *Chem. Eng. Process.: Process Intensif.* **1999**, *38*, 345−353.
(34) Jähnisch, K.; Hessel, V.; Löwe, H.; Baerns, M. *Angew. Chem., Int. Ed.* **2004**, *43*, 406−446.
(35) Hung, L.; Lee, A. P. *J. Med. Biol. Eng.* **2007**, *27*, 1−6.
(36) Kockmann, N.; Kastner, J.; Woias, P. *Chem. Eng. J.* **2008**, *135*, S110−S116.
(37) Song, Y.; Hormes, J.; Kumar, C. S. S. R. *Small* **2008**, *4*, 698−711.